

# Support Information

## Soft Elastomeric Capacitor for Strain and Stress Monitoring on Sutured Skin Tissues

Han Liu,<sup>\*,†</sup> Simon Laflamme,<sup>†,‡</sup> Eric M. Zellner,<sup>¶</sup> Adrien Aertsens,<sup>¶</sup> Sarah A. Bentil,<sup>§</sup> Iris V. Rivero,<sup>||,⊥</sup> and Thomas W. Secord<sup>#</sup>

<sup>†</sup>*Department of Civil, Construction and Environmental Engineering, Iowa State University, Ames, IA, 50011, USA*

<sup>‡</sup>*Department of Electrical and Computer Engineering, Iowa State University, Ames, IA, 50011, USA*

<sup>¶</sup>*Veterinary Clinical Sciences, Iowa State University, Ames, IA, 50011, USA*

<sup>§</sup>*Department of Mechanical Engineering, Iowa State University, Ames, IA 50011, USA;*

<sup>||</sup>*Department of Industrial and Systems Engineering, Rochester Institute of Technology, Rochester, NY 14623, USA;*

<sup>⊥</sup>*Department of Biomedical Engineering, Rochester Institute of Technology, Rochester, NY 14623, USA*

<sup>#</sup>*Department of Industrial and Systems Engineering, University of St. Thomas, St. Paul, Minnesota 55105 USA;*

E-mail: liuhan@iastate.edu

Phone: +1 515 294 2140

# Electromechanical Model

The SEC is meant to be adhered onto the measured substrate (e.g., skin tissue) along the  $x - y$  axis. In what follows, the SEC's electromechanical model characterizing the response of the corrugated SEC under composite effect is derived.

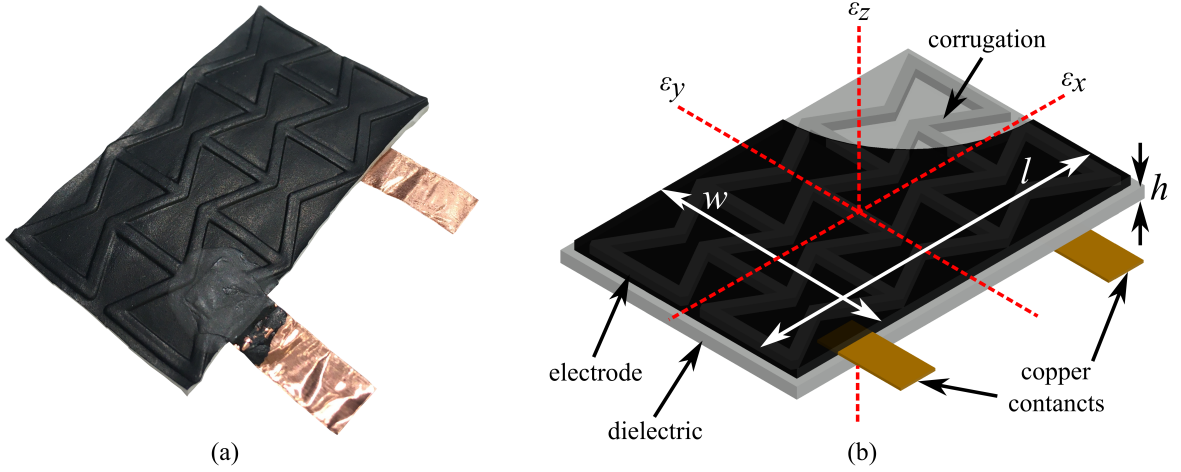


Figure S1: (a) Picture of a 50 mm  $\times$  32 mm corrugated SEC (symmetric reinforced diagrid pattern); and (b) annotated schematic of a corrugated SEC with an effective sensing area  $w \times l$ .

Assuming under a low measurement frequency ( $<1$  kHz), the SEC can be modeled as a non-lossy parallel plate capacitor of initial capacitance  $C_0$ :

$$C_0 = \epsilon_0 \epsilon_r \frac{A}{h} \quad (1)$$

where  $\epsilon_0 = 8.854$  pF/m is the vacuum permittivity,  $\epsilon_r$  is the relative permittivity, and  $A = w \times l$  is the electrode or effective sensing area (Figure S1(b)). By differentiating Eq.1 with respect to the length  $l$  and width  $w$  and applying Hooke's Law under the assumption of plane strain  $\epsilon_x = \Delta l/l$  and  $\epsilon_y = \Delta w/w$ , the capacitance of a free-standing SEC under small strain can be written:

$$\frac{\Delta C}{C_0} = \frac{1}{1 - \nu_0} (\epsilon_x + \epsilon_y) = \lambda_0 (\epsilon_x + \epsilon_y) \quad (2)$$

where  $\Delta C$  is the change in capacitance,  $\nu_0$  is the Poisson's ratio of an non-corrugated (isotropic) SEC, defined as  $\nu_0 = \nu_x = \nu_y = \nu_z$ , and  $\lambda_0$  is the resulting gauge factor. The use of a corrugated surface tunes the in-plane stiffness and creates an orthotropic composite in the  $x - y$  plane, with

$$\nu_{xy} = -\frac{\epsilon_y}{\epsilon_x} \quad (3)$$

Substituting Eq.3 into Eq.2 yields the electromechanical model for a textured SEC under uniaxial strain (along the  $x$ -direction).

$$\frac{\Delta C}{C_0} = \left( \frac{1 - \nu_{xy}}{1 - \nu} \right) \epsilon_x = \lambda \epsilon_x \quad (4)$$

where  $\nu = \nu_{xz} = \nu_{yz}$  is the Poisson's ratio in the  $x - y$  and  $x - z$  planes, corresponding to the Poisson's ratio of the non-corrugated SEC, and  $\lambda$  is the gauge factor in a free-standing (SEC not adhered onto a substrate) configuration.

Eq.4 indicates that the gauge factor of a corrugated SEC is a function of the transverse Poisson's ratio, and  $\lambda$  increases with decreasing  $\nu_{xy}$ . When the SEC is adhered onto a substrate, the gauge factor  $\lambda$  is also influenced by the substrate's stiffness and the level of adhesion SEC-substrate. This creates a composite effect, and in this case  $\lambda$  is taken as

$$\lambda = \frac{1 - \frac{a\nu_{xy} + b\nu_m}{a+b}}{1 - \nu} \quad (5)$$

where  $\nu_m$  is the Poisson's ratio of the substrate, and  $0 \leq a \leq 1$  and  $0 \leq b \leq 1$  are the weight coefficients representing the composite effect with  $a + b = 1$ . For simplicity, these coefficients are combined under the term  $\nu_{xy,c}$  that denotes the composite effect, with Eq.4 becoming

$$\lambda = \frac{1 - \nu_{xy,c}}{1 - \nu} \quad (6)$$

This electromechanical model (Eq. 6) can be used to simulate the electrical response of the sensor in a finite element model (FEM), where the capacitance is obtained by evaluating the change in area of each meshed element located under the SEC, with:<sup>1</sup>

$$\frac{\Delta C}{C_0} = \frac{1}{A_0} \sum_{i=1}^n A_{0i} \left( \frac{A_{li}^2}{A_{0i}^2} - 1 \right) \quad (7)$$

where  $A_0$  is the sensing area under the SEC, and  $A_{0i}$  and  $A_{li}$  are the initial and deformed areas of the  $i_{th}$  mesh element, respectively, extracted from the FEM.

## Skin Specimens

Five canine skin specimens were taken from the lateral aspect of the proximal portion of each pelvic limb of a beagle by using a 10 cm x 10 cm template for demarcating and harvesting to ensure consistency and uniformity of the skin specimen, consistent with the procedure used in,<sup>2</sup> and the dogs were all mature female beagle ranging in weight between 9 to 12 kg. The dimensions of each skin specimen are tabulated in Table S1, and all values are averaged values of three measurements. The harvested specimens have been preserved in an euhydrated state ( $-20\text{ }^{\circ}\text{C}$ ) over one year and soaked in a 0.9% sodium chloride solution for 24 h thawing and the subcutaneous tissue (hypodermis) removed before being utilized. Note that the animal was euthanized for reasons unrelated to this study. Four skin specimens were randomly selected and an approximately 10 cm incision was made throughout the middle the specimens by following a proximal-to-distal orientation, creating the “wounded skin” specimens. The throughout incision was selected in this study to enable the fully sutured in the middle zone of skin specimen and allow a direct evaluation of the suture pattern. These wounded skin specimens were sutured using the various suture patterns described above (Figure 3) using 3-0 poliglecaprone 25 on a reverse-cutting (FS-2) needle. One skin specimens were left intact for benchmarking purposes, yielding a total of 5 canine skin specimens. The skin specimens and suturing process are consistent with work describe in.<sup>2</sup>

Table S1: Geometry dimension of each sutured skin specimens (measured by calliper).

suture pattern	length (mm)	width (mm)	thickness (mm)	gauge length (mm)	section area (mm <sup>2</sup> )
interrupted	96.3	89.4	1.98	71.2	170.0
cruciate	93.1	86.6	2.09	72.9	181.0
intradermal	92.3	88.2	2.03	76.8	179.0
intact	96.7	86.6	1.99	68.8	172.3
pure skin	96.3	86.5	1.90	71.9	164.3

# Experimental Test

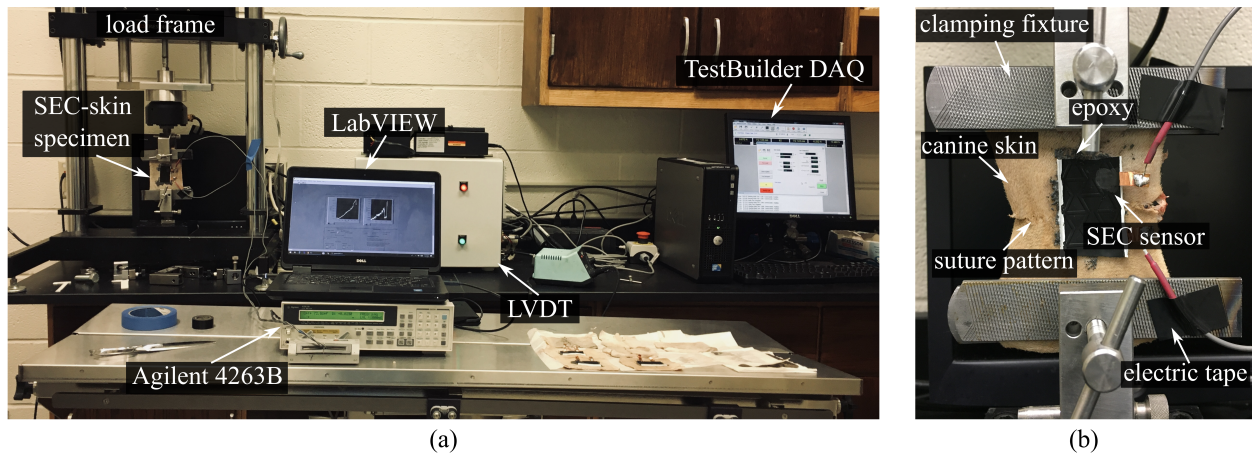


Figure S2: (a) Overall experimental configuration; and (b) zoom on a skin-SEC specimen.

## Constitutive Models

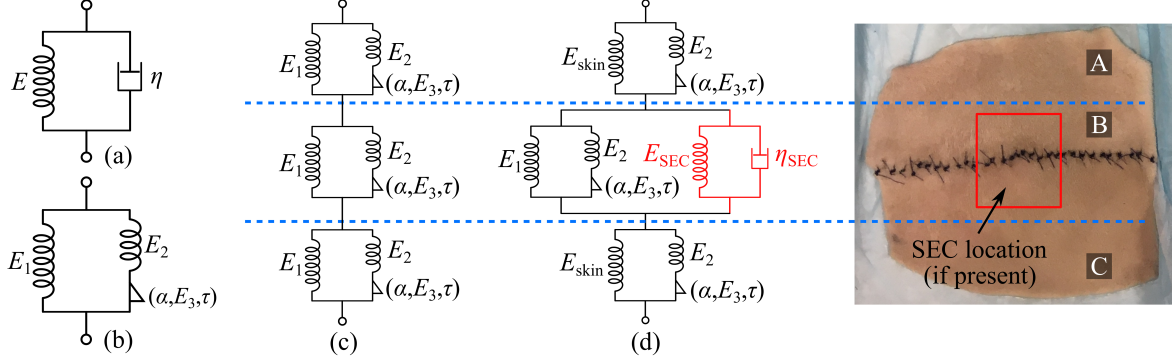


Figure S3: (a) KV model; (b) FZ model where the triangle represents the fractional element; (c) canine skin model without SEC; and (d) skin-SEC model.

Mathematically, the stress function derived from the KV model (Figure S3(a)) can be expressed as:

$$\sigma(t) = E\varepsilon(t) + \eta \frac{d\varepsilon(t)}{dt} = (a + b \cdot e^{c\varepsilon})\varepsilon(t) + (x + y \cdot e^{z\varepsilon}) \frac{d\varepsilon(t)}{dt} \quad (8)$$

where  $\sigma$  is the stress,  $E$  the Young's or elastic modulus,  $\eta$  the viscosity modulus, and  $a$ ,  $b$ ,  $c$ ,  $x$ ,  $y$ , and  $z$  constants used to parameterize the model. The FZ model (Figure S3(b)) is typically used to better explain stress relaxation and creep compliance, useful for some biomechanical materials such as canine skin.<sup>3,4</sup> Its stress function is written

$$\sigma(t) + \tau_0^\alpha D^\alpha \sigma(t) = E_\infty \sigma(t) + E_0 \tau_0^\alpha D^\alpha \varepsilon(t) \quad (9)$$

where  $D^\alpha \sigma(t)$  represents the differintegral of stress at an arbitrary order  $\alpha$  that describes the linear viscoelastic region and can be used to characterize tissue degradation,<sup>3</sup> and with  $E_\infty = E_1$ ,  $E_0 = E_1 + E_2$ ,  $\tau_0^\alpha = (E_3/E_2)\tau^\alpha$ , and  $\tau = \eta/E_2$  describing the stress relaxation time. Substituting these parameters into Eq. 11, one obtains:

$$\sigma(t) + \left(\frac{E_3}{E_2}\right) \left(\frac{\eta}{E_2}\right)^\alpha D^\alpha \sigma(t) = E_1 \sigma(t) + (E_1 + E_2) \left(\frac{E_3}{E_2}\right) \left(\frac{\eta}{E_2}\right)^\alpha D^\alpha \varepsilon(t) \quad (10)$$

Defining elasticity  $E_3$  and viscosity  $\eta$  as a function of strain  $\varepsilon$ , and assigning  $E_2 = l + m \cdot e^{n\varepsilon}$  and  $E_3 = p + q \cdot e^{r\varepsilon}$  for nonlinearities quantification, the stress objective function derived from the FZ model can be written

$$\begin{aligned} \sigma(t) = & (a + b \cdot e^{c\varepsilon})\sigma(t) + (a + b \cdot e^{c\varepsilon}) + (l + m \cdot e^{n\varepsilon}) \left( \frac{p + q \cdot e^{r\varepsilon}}{l + m \cdot e^{n\varepsilon}} \right) \left( \frac{x + y \cdot e^{z\varepsilon}}{l + m \cdot e^{n\varepsilon}} \right)^\alpha D^\alpha \varepsilon(t) \\ & - \left( \frac{p + q \cdot e^{r\varepsilon}}{l + m \cdot e^{n\varepsilon}} \right) \left( \frac{x + y \cdot e^{z\varepsilon}}{l + m \cdot e^{n\varepsilon}} \right)^\alpha D^\alpha \sigma(t) \end{aligned} \quad (11)$$

where  $\alpha$ ,  $l$ ,  $m$ ,  $n$ ,  $p$ ,  $q$ , and  $r$ , are constants. For each FZ element, the overall stiffness  $E_{\text{FZ}}$  and viscosity  $\eta_{\text{FZ}}$  are

$$\frac{1}{E_{\text{FZ}}} = \frac{1}{E_1} + \frac{E_2 + E_3}{E_2 \cdot E_3} \quad (12)$$

$$\frac{1}{\eta_{\text{FZ}}} = \frac{1}{\tau E_2} \quad (13)$$

For the FZ models arrangement used to characterize wounded or sutured skin (Figure S3(c), where parameter values are not necessarily constant across all FZ elements), these expressions become

$$E_{\text{FZ-skin}} = \frac{1}{\frac{1}{E_{\text{FZ}}}|_A + \frac{1}{E_{\text{FZ}}}|_B + \frac{1}{E_{\text{FZ}}}|_C} \quad (14)$$

$$\eta_{\text{FZ-skin}} = \frac{1}{\frac{1}{\eta_{\text{FZ}}}|_A + \frac{1}{\eta_{\text{FZ}}}|_B + \frac{1}{\eta_{\text{FZ}}}|_C} \quad (15)$$

where  $|$  indicates the FZ-element at the location indicated by the subscript (see picture in Figure S3). The expression can be specialized for the case of intact skin, where all FZ elements are parameterized equally, yielding

$$E_{\text{FZ-skin}} = 3 \cdot E_{\text{FZ}} \quad (16)$$

$$\eta_{\text{FZ-skin}} = 3 \cdot \eta_{\text{FZ}} \quad (17)$$

Finally, for constitutive model characterizing the skin-SEC dynamics (Figure S3(d)), the overall stiffness  $E_{\text{skin-SEC}}$  and viscosity  $\eta_{\text{skin-SEC}}$  are written

$$E_{\text{skin-SEC}} = \frac{1}{\frac{1}{E_{\text{FZ}}}\Big|_A + \frac{1}{E_{\text{eff}}}\Big|_B + \frac{1}{E_{\text{FZ}}}\Big|_C} \quad (18)$$

$$\eta_{\text{skin-SEC}} = \frac{1}{\frac{1}{\eta_{\text{FZ}}}\Big|_A + \frac{1}{\eta_{\text{eff}}}\Big|_B + \frac{1}{\eta_{\text{FZ}}}\Big|_C} \quad (19)$$

with

$$\frac{1}{E_{\text{eff}}}\Big|_B = \frac{1}{E_{\text{FZ}}}\Big|_B + \frac{1}{E_{\text{SEC}}} \quad (20)$$

$$\frac{1}{\eta_{\text{eff}}}\Big|_B = \frac{1}{\eta_{\text{FZ}}}\Big|_B + \frac{1}{\eta_{\text{SEC}}} \quad (21)$$

giving

$$E_{\text{SEC}} = \frac{-(3 \cdot E_{\text{skin-SEC}} - E_{\text{FZ}})E_{\text{FZ}}}{2 \cdot E_{\text{skin-SEC}} - E_{\text{FZ}}} \quad (22)$$

$$\eta_{\text{SEC}} = \frac{-(3 \cdot \eta_{\text{skin-SEC}} - \eta_{\text{FZ}})\eta_{\text{FZ}}}{2 \cdot \eta_{\text{skin-SEC}} - \eta_{\text{FZ}}} \quad (23)$$

with  $E_{\text{FZ}}\Big|_A = E_{\text{FZ}}\Big|_C = E_{\text{FZ}}$  and  $\eta_{\text{FZ}}\Big|_A = \eta_{\text{FZ}}\Big|_C = \eta_{\text{FZ}}$ . The total stress in the skin-SEC specimen at the location of the sensor (zone 'B' in Figure S3)  $\sigma_{\text{skin-SEC}}$  is the summation of the stress at the skin ( $\sigma_{\text{skin}}$ ) and sensor ( $\sigma_{\text{SEC}}$ ) level.

## FEM Validation

The validation of the FEM was conducted by comparing experimental to numerical results obtained from a skin-SEC specimen, with the skin intact and a honeycomb patterned corrugation. First, the validation of the biomechanical response was conducted by comparing experimental and numerical axial force measurements from both quasi-static and dynamic cyclic tests. The numerical values were obtained by assigning experimental strain input to the numerical model. The axial force are plotted against axial strain in Figure S4(a) under quasi-static load. There is a good fit between the experimental and numerical results, with an overall root mean square errors (RMSE) of 6.68% and 9.01% under quasi-static and dynamic loads. The noticeable discrepancies at low strain levels can be attributed to plastic deformations inducing slack in the specimens, which can be confirmed by the decreasing peak force over each cycle. When evaluating all corrugation patterns, the RMSE remains in the range of 3-9% and 7-10% under quasi-static and dynamic loads, respectively.

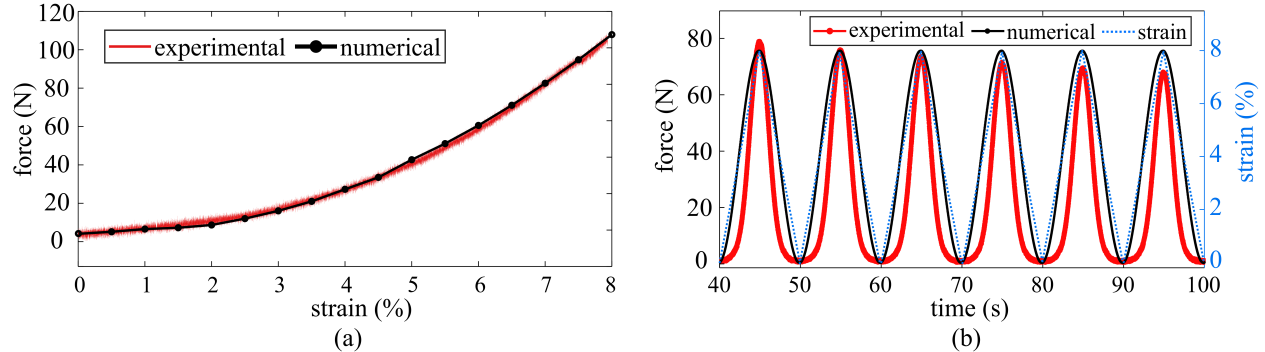


Figure S4: Comparison of experimental and numerical axial forces under (a) quasi-static; and (b) dynamic loads.

Second, the validation of the simulated electrical signal was conducted by comparing results to the experimentally measured capacitance. The simulations were conducted on the same FEM validated above, and the numerical capacitance signal obtained using Eq.7. Figures S5(a) and (b) compares typical results under the quasi-static and dynamics loads, respectively, for the skin-SEC (intact-honeycomb) specimen. There is good agreement between experimental and numerical results, with the RMSE remaining in the range of 4-6%

and 5-7% respectively under quasi-static and dynamic loads over all sensor patterns. Discrepancies in the time series plotted in Figures S4(b) and S5(b) can be attributed to local plastic deformations in the canine skin, the stress relaxation process,<sup>5</sup> and softer bonds caused by the adiabatic heating effect.<sup>6</sup> Overall, results indicate that the FEM can be used to simulate the skin-SEC specimens.

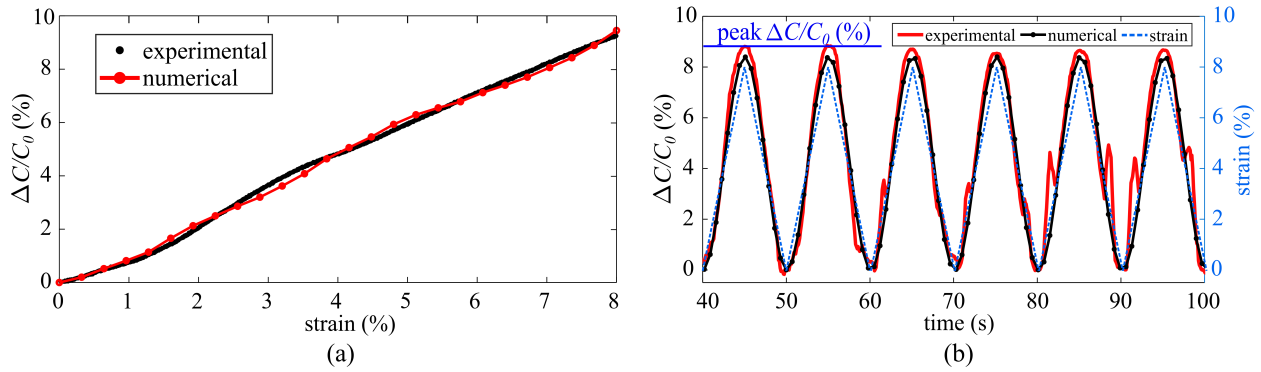


Figure S5: Comparison of experimental and numerical signal  $\Delta C/C_0$  under (a) quasi-static; and (b) dynamic loads.

## FZ Parameter

Table S2 lists the optimal parameters used for the constitutive models under each suture pattern. The  $\alpha$  values for the pure (no SEC) and intact skins are lower than for the sutured skin, which implies that unwounded skin behaves more like an elastic solid.

Table S2: Particle Swarm Algorithm (PSA) obtained parameter values used in the constitutive models to estimate stress on the 'skin-SEC' specimens at the ROI

	$\alpha$	$E_1$ (Pa)			$E_2$ (Pa)			$E_3$ (Pa)			$\eta$		
		$a$	$b$	$c$	$l$	$m$	$n$	$p$	$q$	$r$	$x$	$y$	$z$
pure skin_static	0.38	3516	7971	82	6523	1340	34	668	9123	85	612	5183	42
pure skin_dynamic	0.38	2519	8601	70	4213	713	38	4111	8052	83	3835	4281	40
skin-SEC_static $\sigma_{\text{skin}}$	0.40	4279	478	96	9216	1692	46	492	5003	88	6139	468	69
skin-SEC_static $\sigma_{\text{SEC}}$	-	789	6132	66	-	-	-	-	-	-	520	3306	20
skin-SEC_dynamic $\sigma_{\text{skin}}$	0.41	985	2110	85	9260	2051	33	8353	8213	80	8112	3460	39
skin-SEC_dynamic $\sigma_{\text{SEC}}$	-	15	809	33	-	-	-	-	-	-	4426	353	21
interrupted $\sigma_{\text{skin}}$	0.43	3473	64322	34	3080	582	42	3422	47052	66	1703	425	48
interrupted $\sigma_{\text{SEC}}$	-	311	1862	58	-	-	-	-	-	-	4426	5080	62
cruciate $\sigma_{\text{skin}}$	0.46	4802	39413	21	2008	2526	34	3289	60081	61	5923	425	63
cruciate $\sigma_{\text{SEC}}$	-	2539	6734	49	-	-	-	-	-	-	2102	8611	59
intradermal $\sigma_{\text{skin}}$	0.48	1831	52016	26	366	3013	40	893	36996	64	253	1526	49
intradermal $\sigma_{\text{SEC}}$	-	117	3641	60	-	-	-	-	-	-	4831	8823	61

## References

- (1) Kong, X.; Li, J.; Bennett, C.; Collins, W.; Laflamme, S. Numerical simulation and experimental validation of a large-area capacitive strain sensor for fatigue crack monitoring. *Measurement Science and Technology* **2016**, *27*, 124009.
- (2) Zellner, E. M.; Hedlund, C. S.; Kraus, K. H.; Burton, A. F.; Kieves, N. R. Comparison of tensile strength among simple interrupted, cruciate, intradermal, and subdermal suture patterns for incision closure in ex vivo canine skin specimens. *Journal of the American Veterinary Medical Association* **2016**, *248*, 1377–1382.
- (3) Ciniello, A. P. D.; Bavastri, C. A.; Pereira, J. T. Identifying Mechanical Properties of Viscoelastic Materials in Time Domain Using the Fractional Zener Model. *Latin American Journal of Solids and Structures* **2017**, *14*, 131–152.
- (4) Yang, S.-M.; Duan, J.-S. Response analysis of six-parameter fractional constitutive model. *Physica Scripta* **2020**, *96*, 025220.
- (5) Liber-Kneć, A.; Łagan, S. The Stress Relaxation Process in Sutures Tied with a Surgeon's Knot in a Simulated Biological Environment. *Polymers in Medicine* **2017**, *46*, 111–116.
- (6) Soares, G. C.; Patnamsetty, M.; Peura, P.; Hokka, M. Effects of Adiabatic Heating and Strain Rate on the Dynamic Response of a CoCrFeMnNi High-Entropy Alloy. *Journal of Dynamic Behavior of Materials* **2019**, *5*, 320–330.